Vol. 56: 181–196, 2013
doi: 10.3354/cr01152

CLIMATE RESEARCH
Clim Res

Published online April 24

Downscaling reanalysis over continental Africa with a regional model: NCEP versus ERA Interim forcing

Leonard M. Druyan[1,2,*], Matthew Fulakeza[1,2]

[1]Center for Climate Systems Research, Columbia University, and
[2]NASA/Goddard Institute for Space Studies, 2880 Broadway, New York, New York 10025, USA

ABSTRACT: Five annual climate cycles (1998–2002) are simulated for continental Africa and adjacent oceans by a regional atmospheric model (RM3). RM3 horizontal grid spacing is 0.44° at 28 vertical levels. Each of 2 simulation ensembles is driven by lateral boundary conditions from each of 2 alternative reanalysis data sets. One simulation downscales National Center for Environmental Prediction reanalysis 2 (NCPR2) and the other the European Centre for Medium Range Weather Forecasts Interim reanalysis (ERA-I). NCPR2 data are archived at 2.5° grid spacing, while a recent version of ERA-I provides data at 0.75° spacing. ERA-I-forced simulations are recommended by the Coordinated Regional Downscaling Experiment (CORDEX). Comparisons of the 2 sets of simulations with each other and with observational evidence assess the relative performance of each downscaling system. A third simulation also uses ERA-I forcing, but degraded to the same horizontal resolution as NCPR2. RM3-simulated pentad and monthly mean precipitation data are compared to Tropical Rainfall Measuring Mission (TRMM) data, gridded at 0.5°, and RM3-simulated circulation is compared to both reanalyses. Results suggest that each downscaling system provides advantages and disadvantages relative to the other. The RM3/NCPR2 achieves a more realistic northward advance of summer monsoon rains over West Africa, but RM3/ERA-I creates the more realistic monsoon circulation. Both systems recreate some features of July–September 1999 minus 2002 precipitation differences. Degrading the resolution of ERA-I driving data unrealistically slows the monsoon circulation and considerably diminishes summer rainfall rates over West Africa. The high resolution of ERA-I data, therefore, contributes to the quality of the downscaling, but NCPR2 lateral boundary conditions nevertheless produce better simulations of some features.

KEY WORDS: Regional climate models · West African monsoon · Lateral boundary conditions · Reanalysis

1. INTRODUCTION

Africa is a priority region for improving assessments of climate change. The Intergovernmental Panel on Climate Change (IPCC) 4th Assessment Report (IPCC 2007) emphasized that 'Africa is one of the most vulnerable continents because of the range of projected impacts, multiple stresses and low adaptive capacity.' However, IPCC 4th Assessment climate change prediction models have not produced consensus about how water availability in West Africa (WA) will change toward the end of the 21st century (Druyan 2011). Since societal sustainability of many African regions is acutely sensitive to climate, reliable projections of climate trends would be valuable for mitigating negative impacts. Confidence in climate change projections is often judged by a model's skill in simulating observable contemporary climate variability. Effective spatial representation of climate features can be achieved by using regional climate models (RCMs) to downscale coarse grid global analyses or projections. Lateral boundary conditions (LBCs) from global data sets supply the information that distinguishes an RCM simulation of one

*Email: ldruyan@giss.nasa.gov

year from another. The present study examined RCM downscaling experiments over Africa with 3 alternative sets of LBCs. It considered the relative merits of each downscaled climate and therefore the sensitivity of the RCM product to the forcing analysis.

The mesoscale spatial resolution of RCMs contributes to more realistic simulations of climate systems and processes that are relevant to hydrological trends. For example, RCM simulations of transient synoptic African Easterly Waves and associated mesoscale squall lines over WA provide useful spatial detail (Druyan et al. 2006, 2008). More recently, Lim et al. (2011) demonstrated that downscaling National Center for Environmental Prediction reanalysis 2 (NCPR2) (Kanamitsu et al. 2002) with an RCM on a 20 km computational grid yields a mean summertime precipitation distribution with additional spatial detail and in better agreement with observations than NCPR2 precipitation. Denis et al. (2002) evaluated advantages of RCM downscaling to a 45 km grid (over eastern North America), based on a so-called 'big brother' approach, which assesses RCM improvements in spatial and temporal variability compared to the forcing data. Denis et al. (2002) concluded that 1-way nesting strategy indeed has skill in downscaling large-scale information to regional scales. Moreover, the time mean and variability of several fine-scale climate parameters are successfully reproduced, particularly over regions where mesoscale surface forcings are strong. Improvements over the ocean and away from the surface are less impressive. Haensler et al. (2011) investigated the capability of the REMO RCM to simulate mesoscale climate patterns over southern Africa, with focus on SW Africa. The simulations were conducted by double-nesting, with an inner grid spacing of about 18 km, for the period 1958–2007. The outermost lateral boundary forcing is from ERA40 (European Centre for Medium-Range Weather Forecasts 40-year reanalysis) and other operational analysis data. The study found that RCM results agree rather well with observations of spatial and temporal variability. For example, REMO seasonal precipitation characteristics and the inter-annual rainfall variability for the SW Africa focus region are very close to observations. A distinct added value is achieved, compared to the ERA40 forcing data, in the form of a significantly better representation of the seasonal rainfall amounts around the southern African cape region. Some REMO deficiencies are noted, however, in the simulation of the 2 m air temperature. The current study used forcing from ERA-interim reanalysis (ERA-I), gridded at 0.75°, an improved representation of actual climate variability compared to ERA40, according to Sylla et al. (2010).

Paeth & Thamm (2007) studied the effects of greenhouse warming and land degradation on African precipitation using REMO 1 yr time slice regional model simulations on a 0.5° grid forced by ECHAM4/HOPE global model of the IPCC B2 projections up to 2025. They found that projected strengthening of summer monsoon circulation from increases in continental surface heating is more than offset by decreases in evapotranspiration from reduced vegetation and soil degradation. Lower evapotranspiration in the simulations inhibits moist convection, promoting drought, especially during summer in the Sahel. In a related examination, Steiner et al. (2009) showed that RCM simulations of the WA summer monsoon are sensitive to the model's land surface/hydrology scheme. In particular, coupling of the Community Land Model (CLM3) to the RegCM3 regional climate model substantially improves the simulation of mean climate over WA relative to an older version of RegCM3 coupled to the Biosphere Atmosphere Transfer Scheme (BATS). Two 10 yr simulations (1992–2001) show that the seasonal timing and magnitude of mean monsoon precipitation more closely match observations when the new land surface scheme is implemented. RegCM3–CLM3 improves the timing of the monsoon advance and retreat across the Guinean Coast, and reduces a positive precipitation bias in the Sahel and northern Africa.

Sylla et al. (2010) examined the ability of a recent version of the RegCM3 regional climate model to reproduce seasonal mean climatology, annual cycle and interannual variability over the entire African continent and different climate sub-regions. The 0.75° ERA-I was used to provide initial conditions and LBCs for the RegCM3 simulation. The RegCM3 was integrated over Africa continuously for 17 yr (January 1989 through December 2005) at a spatial resolution of 50 km. The mean annual cycle of precipitation was simulated well, including single and multiple rainy seasons, as well as the observed interannual variability of precipitation over most African sub-regions, in some cases even improving the quality of the ERA-I precipitation product. Sylla et al. (2011) also used the RegCM3 forced by ERA-I in a sensitivity study over WA and southeastern North Atlantic. Two 5 yr simulations of the summer monsoon were made with and without deep convection to evaluate the impact of the latter on the West African monsoon (WAM) climate. The current study tested the sensitivity of RCM simulations over Africa to alternative boundary forcing, also in a series of 5 yr runs.

The Coordinated Regional Downscaling Experiment (CORDEX) is sponsored by the World Climate Research Program (WCRP). CORDEX anticipates downscaling atmosphere–ocean global climate models (AOGCM) projections of decadal climate change (Jones et al. 2011) using RCMs, and Africa is the highest priority region. CORDEX RCM projections of climate change are planned for inclusion in the next assessment report (AR5) of the IPCC. An initial step would be to evaluate model performance in simulating the contemporary climate based on forcing from ERA-I, 1989–2008. Preliminary CORDEX-related results of RCM simulations over Africa have been published by Nikulin et al. (2012) and Hernandez-Diaz et al. (2013). The selection of ERA-I to drive regional simulations of the contemporary climate implies confidence in its representation of atmospheric evolution relative to other available data sets. Some of the advances represented by ERA-I, the third generation ECMWF reanalysis product, reflect its higher resolution and improved model physics, as summarized by Sylla et al. (2010).

Thorncroft et al. (2011) described the following major stages in the annual WA precipitation cycle based on ERA-I data, 1989–2009: (1) an oceanic phase between November and mid-April, when the rain band is broad with peak values just north of the Equator; (2) a coastal phase between mid-April and the end of June, when the rainfall peak is in the coastal region around 4° N (over the ocean); (3) a transitional phase during the first half of July, when the rainfall peak decreases; and (4) a Sahelian phase between mid-July and September when the rainfall peak is more intense and established in the Sahelian region around 10° N. Earlier, Gu & Adler (2004) documented the break in WA rainfall during Phase 3.

Nikulin et al. (2012) showed the annual cycle of area averaged, 1998–2008 precipitation rates simulated by 10 CORDEX participating regional models forced by ERA-I. These were compared with corresponding TRMM rates and corresponding rates from the ERA-I data set. Results over northern WA are averages over 7.5–15° N, 10° W–10° E. Individual RCM simulations show a wide spread around the observed annual cycle, with several overestimates and underestimates during the development and maximum phase of the WAM. Much better agreement is seen between the RCMs and observations during the decay of the rainy season (October–November). Overestimates during the onset represent a premature start of the rainy season in many RCMs, by as much as a whole month. Their ensemble mean reproduces the common tendency of the RCMs to overestimate precipitation during the onset, but it otherwise accurately represents the observed annual cycle. Several RCMs, and particularly the ensemble mean, improve on ERA-I, which has a large dry bias during the rainy season. Druyan et al. (2010) also found excessive peak Sahel rainfall to be simulated by regional models compared to the rates produced by the driving model. More recently, Hernandez-Diaz et al. (2013) showed that the Canadian Regional Climate Model (CRCM5) summer precipitation rates over the same northern WA area studied by Nikulin et al. (2012) are some 40% lower than observations. They attribute the CRCM5 deficiency to an equatorward displacement of the simulated Sahara heat low and, consequently, the WAM rain band.

The present study evaluated the performance of ERA-I for driving an RCM over Africa, relative to using NCPR2 (Kanamitsu et al. 2002) forcing. A recent version of ERA-I provided data at a 0.75° grid spacing, while NCPR2 data were archived at 2.5° spacing. One motivation for the study was that the high resolution of ERA-I is more resource intensive than other lower resolution global analyses, so its benefits should be tangible. In addition, it is useful for evaluating and quantifying the sensitivity of RCM performance to differences in alternative reanalysis data sets or other forcing that may be used for LBCs. Impacts may be a consequence of the resolution of the forcing data or its intrinsic quality. The RCM in this study was the RM3, described in the next section. Note that much of the development of the RM3 has been based on NCPR1- and NCPR2-forced simulations (for example, Druyan et al. 2008).

2. THE REGIONAL MODEL

The RM3 is a third generation version atmospheric model developed and run at the Center for Climate Systems Research (Columbia University) and the Goddard Institute for Space Studies (CCSR/GISS). The RM3 is integrated at 28 vertical sigma levels on a horizontal grid with 0.44° spacing. The domain, 49.5° S–49.5° N, 35° W–64° E, covers all of Africa, the eastern Atlantic Ocean, the western Indian Ocean and southern Europe. Druyan et al. (2008) described the RM3 for applications over WA. It uses the same land surface (LS) process model as that in the GISS GCM (Rosenzweig & Abramopoulos 1997, Hansen et al. 2002). The LS model consists of 2 integrated parts, the soil and the canopy, and it conserves water and heat, while simulating their vertical fluxes. The RM3 modeled soil is divided into 6 lay-

ers to a depth of 3.5 m, and the model distinguishes between 5 textures of soil. The canopy, modeled as a separate layer located above the soil, is responsible for the interception of precipitation, evaporation of accumulated water and removal of soil water through transpiration.

The RM3 uses the DelGenio & Yao (1993) moist convection parameterization and the Del Genio et al. (1996) scheme for the effects of cloud liquid water. These are components originally developed for the GISS global climate model, which itself has been extensively applied to climate sensitivity studies (e.g. Hansen et al. 2002) and has been used in the 4th Assessment of the IPCC. The cloud liquid water scheme allows for life-cycle effects in stratiform clouds and permits cloud optical properties to be determined interactively.

3. SIMULATIONS

Each of 2 sets of simulations was initialized at 00 UT on 30 November in consecutive years, 1997–2001, and simulations were extended to cover entire calendar years, January–December, 1998–2002. Ensemble means of the 1998–2002 simulations were evaluated, as well as interannual variability and climate features of particular years. The year 1998 is the earliest for which Tropical Rainfall Measuring Mission (TRMM) (Huffman et al. 2007) data is available, so 1998 was selected as the first of 5 yr for the current test of sensitivity to LBCs. According to the rain gauge index given by Lélé & Lamb (2010) — which is based on data between 11 and 18° N, west of 10° E — 1999 was the wettest year since the 1960s, experiencing a July–September (JAS) departure of +133% of the JAS 1941–2000 mean. In 2002, the region registered a precipitation deficit of 37% of the 1941–2000 mean. The years 2000 and 2001 did not experience extreme precipitation anomalies, but 1998 was rainier than normal, with a departure of +79% from the base period mean. Thus, 1998–2002 represented a wide range of Sahel precipitation climatologies.

The control simulation was forced by LBCs from ERA-I (0.75° grid), while the second simulation was forced with synchronous NCPR2 data gridded horizontally at 2.5°. LBCs from each reanalysis were interpolated horizontally and vertically to the boundaries of the regional model grid 4 times daily, and corresponding reanalysis sea-surface temperatures were used as the lower boundary condition. RM3 soil moisture was also initialized from each reanalysis at 00 UT on 30 November, 1997–2001. This means that January output has a 1 mo spin-up and June–September results represent a 6 mo spin-up. A third simulation was designed to test the relative influences of LBC resolution versus intrinsic differences between ERA-I and NCPR2. This experiment was driven by ERA-I LBCs that were interpolated to the NCPR2 2.5° horizontal grid. The impact of degrading the resolution of ERA-I was evaluated for the June–September (JJAS) portion of the annual cycle, so this simulation was initialized from the control on each 1 May, 1998–2002, and it extended only to 6 October. Throughout the paper, these simulations will be referred to as: (1) the 'control' (or RM3/ERA-I), (2) 'RM3/NCPR2' and (3) 'RM3/ERAdegr.'

4. RESULTS

4.1. Precipitation

RM3-simulated monthly precipitation rates for 1998–2002 are here compared to TRMM gridded data at 0.5° spacing. Fig. 1 shows time series of RM3/ERA-I, RM3/NCPR2 and RM3/ERAdegr monthly means plotted against TRMM, averaged over the northern WA area identified by Nikulin et al. (2012) bound approximately by 7.5–15° N, 10° W–10° E. TRMM monthly precipitation rates in this region increased from near zero in January, peaked at 7.3 mm d^{-1} in August, then fell sharply to near zero by December. The 12 mo RM3 precipitation time series

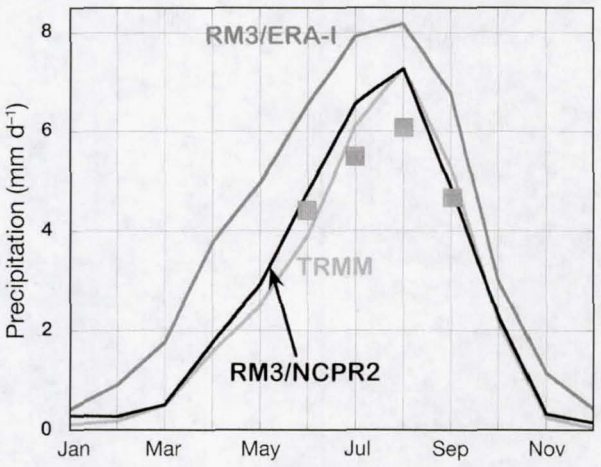

Fig. 1. Time series of RM3/ERA-I and RM3/NCPR2 5 yr, monthly mean precipitation plotted against corresponding tropical rainfall measuring mission (TRMM) estimates, averaged over northern West Africa, bounded by 7.5–15° N, 10° W–10° E. Squares: corresponding June, July, August and September (JJAS) 5 yr mean precipitation for RM3/ERAdegr

had the same shape as TRMM. RM3/ERA-I rainfall rates were rainier than TRMM throughout the year, with an excess of about 12% in August. The corresponding RM3/NCPR2 time series was almost a perfect reproduction of TRMM, showing minimal bias during all months. Degrading the resolution of ERA LBCs created a reduction in northern WA area control run precipitation during each summer month, June–September, ranging between 26 and 32%. This simulation's JJAS precipitation rates were also about 12% lower than those for RM3/NCPR2.

The northward migration of the tropical rain belt between January and August was reflected in the August minus January differences in monthly mean precipitation rate for TRMM (Fig. 2A), RM3/ERA-I (Fig. 2B) and RM3/NCPR2 (Fig. 2C). Positive difference maxima in the northern hemisphere, such as over WA and the eastern tropical Atlantic, indicated the northernmost position in August of the WAM rain band, while negative centers along 3° N over the Atlantic and over southern hemisphere Africa and the western South Indian Ocean denoted January precipitation maxima vacated by the northward shift of the rain band. Both simulations created these main bands of positive and negative differences denoted by the TRMM data. The RM3/ERA-I swath of positive differences was correctly aligned along 8–10° N, with realistic maxima, although the excess over the Atlantic was too low, and near 5° E it was somewhat too high. Moreover, the western lateral boundary adversely effected this maximum between 30 and 35° W in both simulations. RM3/NCPR2 positive differences over the Atlantic ITCZ were similar to RM3/ERA-I. The positive swath over WA in Fig. 2C was correctly narrower than in the control, and the orographic excess over the Cameroon Highlands was also closer to TRMM. Summertime orographic precipitation, appearing as maximum positive differences near the Guinea coast of southwestern WA was simulated realistically by both experiments as were the negative differences over the southern hemisphere.

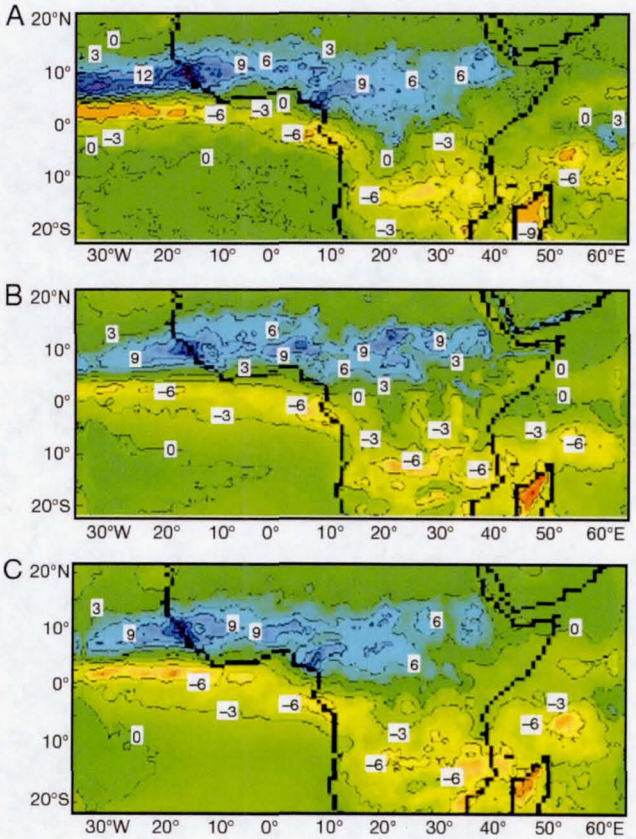

Fig. 2. August minus January differences in 5 yr monthly mean precipitation rates (mm d^{-1}). (A) TRMM, (B) RM3/ERA-I and (C) RM3/NCPR2

As mentioned, JAS 1999 was much rainier over WA than JAS 2002 (Lélé & Lamb 2010). We analysed whether the simulations capture this interannual variability. Fig. 3 shows TRMM and RM3 JAS 1999 minus JAS 2002 precipitation differences. TRMM JAS 1999 excesses were 200 to 400 mm over much of the Sahel, exceeded 400 mm along the Atlantic coast, the Cameroon coast and parts of the western Indian Ocean and ranged between 200 and 400 mm over the Ethiopian Highlands (Fig. 3A). CRU (Climate Research Unit of the University of East Anglia; Mitchell & Jones 2005) precipitation data (not shown), based on rain gauges, showed JAS 1999 minus JAS 2002 difference patterns (over land) to be consistent with TRMM. Fig. 3B shows that RM3/ERA-I corresponding differences were generally less extreme than for TRMM, but nevertheless captured many spatial features of the observed difference pattern. In particular, Fig. 3B indicates positive differences over the Sahel, over a segment of the Atlantic coast and along the Cameroon coast, over the Ethiopian Highlands and over the western Indian Ocean. It also shows some of the observed negative differences over WA between 7 and 10° N. Strong interannual differences not captured by RM3/ERA-I included TRMM excesses along 4–5° N over the Atlantic and the broad area of deficits over the Cameroon Highlands. The last 2 features, however, were reproduced better with NCPR2 forcing (Fig. 3C). While positive differences simulated by RM3/ERA-I along 20° N slightly exaggerated the observed signal, RM3/NCPR2 produced differences that were too moderate over WA and over Ethiopia.

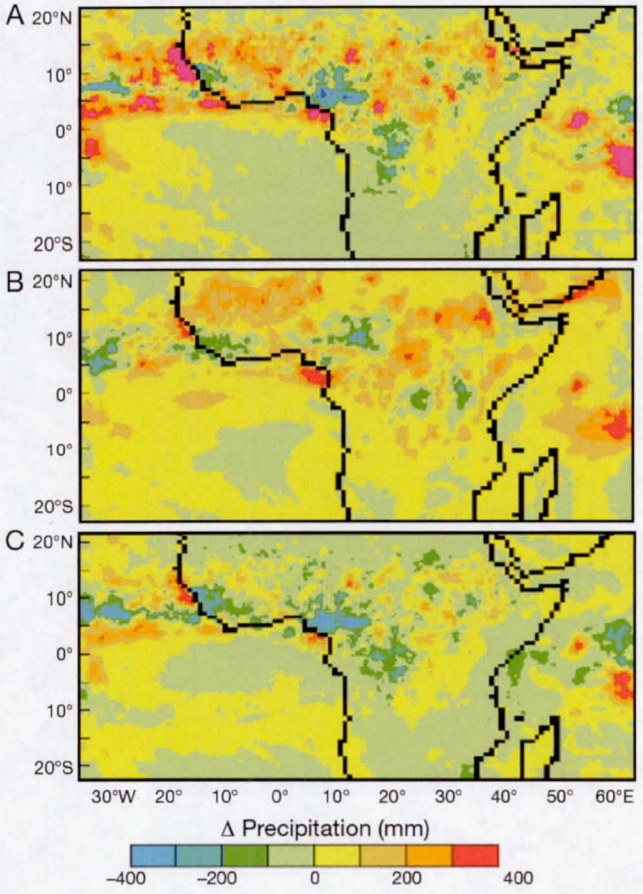

Fig. 3. Precipitation differences, June, August and September (JAS) 1999 minus JAS 2002. (A) TRMM, (B) RM3/ERA-I and (C) RM3/NCPR2

Mean 1998–2002 pentads of TRMM precipitation rates from 1 June were averaged over the longitudes 10° W–10° E and plotted on time versus latitude axes (Fig. 4A) covering 1 June to 28 September. Despite the averaging over 5 seasons, the time–latitude plot shows a rather distinct transition of the rain belt between 4° and 10° N (onset). In particular, rather heavy precipitation lingered over 4° N until the eighth pentad (6 to 10 July) followed by the appearance of a maximum at 10° N in the tenth pentad (16 to 20 July). Lavaysse et al. (2009) suggested a mean onset of WAM rainfall on 25 June, based on records for 1984–2001. The TRMM rain belt axis in Fig. 4A remained near 10° N during the rest of the summer, but it weakened in September (after the 19th pentad).

Fig. 4B shows that the RM3/ERA-I 5 yr ensemble simulated a precipitation maximum between 4 and 6° N during June that was still present in the seventh pentad. Contrary to TRMM observations, the control ensemble also produced a precipitation maximum along 10° N from the beginning of June. This unrealistic feature of pre-onset precipitation near 10° N was apparently a common error in RCMs modeling WAM, as reported in the RCM comparison studies of Druyan et al. (2010) and Nikulin et al. (2012). The control ensemble mean pentads maintained the precipitation maximum near 10° N for the remainder of the summer, and correctly showed the southern edge of the rain belt spreading southward in September. The model ensemble precipitation maximum was about 25% higher than TRMM during July to August and up to 50% higher in September. During midsummer, the RM3 spread heavy rain too far north over the Sahel.

The unrealistic feature of early June rainfall simulated by RM3/ERA-I along 10° N was absent only in the 1998 simulation (not shown), which reproduced TRMM precipitation maxima for 1998 near 3 to 5° N until the ninth pentad (11 to 15 July), followed by a new maximum near 11° N in the tenth pentad. Thus, the multi-year dynamic downscaling of reanalysis encompassed a range of skill that may be related to the quality of the forcing data.

In contrast to RM3/ERA-I results, the RM3 simulations forced by NCPR2 (Fig. 4C) correctly avoided a 10° N maximum until the eighth pentad (6 to 10 July) and correctly maintained the 5° N maximum until the ninth pentad (11 to 15 July). A distinct break in the precipitation maximum identified with monsoon onset (Gu & Adler 2004) occurred in the ninth pentad in TRMM data and in the tenth pentad in RM3/NCPR2 data (Fig. 4A,C). Fig. 4B does not show the break for the RM3/ERA-I simulations. In addition, RM3/NCPR2 July to August pentad maxima along 10° N agreed quite well with TRMM, although the rain band was still too wide, judging by the meridional range of the 6 mm d^{-1} isohyet.

Pentad results for RM3/ERAdegr (Fig. 4D) showed a gradual northward migration of the rain maximum during July, with the break occurring at Pentad 11, some 10 d later than for TRMM. Degrading the resolution of ERA-I LBCs produced an even more unrealistic migration of the summer rain band, which established a very weak midsummer maximum along 10° N and produced too much August precipitation between 5 and 10° N. ERA-I forcing and low resolution combined to degrade the simulation of the onset. On the other hand, despite low resolution, NCPR2 LBCs drove a very realistic onset sequence.

Transient African Easterly Waves (AEWs) organize precipitation maxima over WA throughout the summer, which move westward in tandem with the waves. Accordingly, Xue & Shukla (1993) referred to

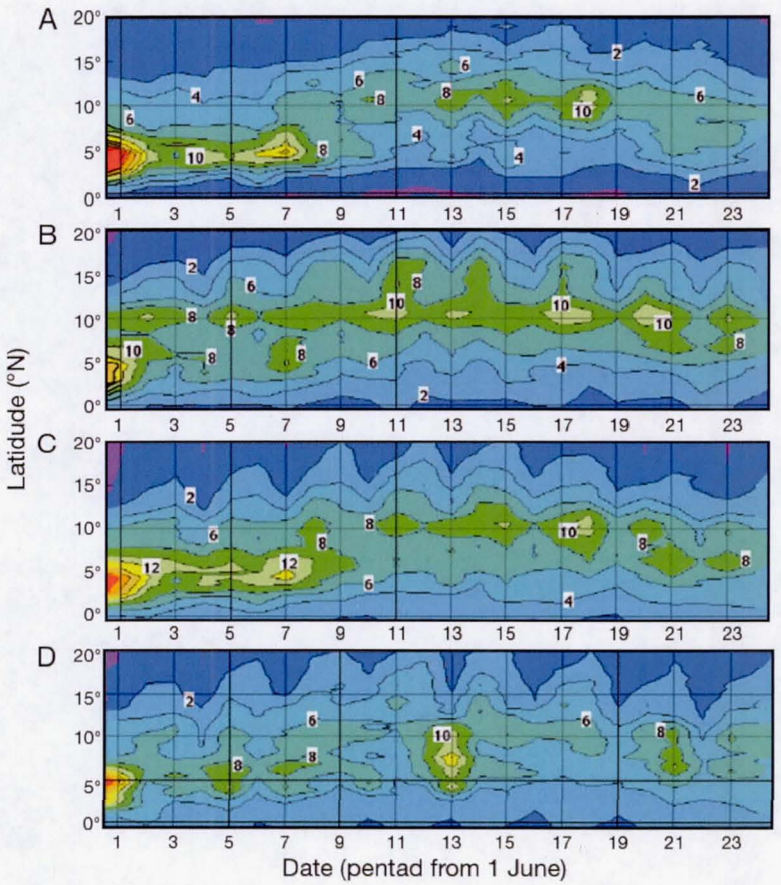

Fig. 4. Time versus latitude distribution of 1998–2002 pentad mean precipitation rates (mm d^{-1}) from 1 June, averaged over the longitudes 10° W–10° E. (A) TRMM, (B) RM3/ERA-I, (C) RM3/NCPR2 and (D) RM3/ERAdegr

diagonal swaths of model-simulated precipitation maxima in a time–longitude Hovmöller distribution as 'footprints' of AEWs, moving east to west across WA. The swaths are represented by maxima separated by lighter precipitation. Druyan et al. (2006) showed such diagonal swaths of TRMM-observed precipitation maxima during June to September 1998, presumably also associated with westward-propagating AEWs. Druyan & Fulakeza (2012) showed that the swaths appear narrower when represented by TRMM 3 h resolution data. We analysed how well these precipitation footprints are simulated by RM3 and how different they are with NCPR2 forcing compared to ERA-I forcing. Fig. 5A–D shows time–longitude Hovmöller distributions of daily TRMM and RM3 simulated precipitation, the latter using each of the 3 sets of LBCs, for the interval 30 July to 8 September 2002. Daily accumulations at the designated longitudes were averaged over the width of the rain band between 5 and 15° N. RM3/ERA-I and RM3/NCPR2 simulated all of the precipitation swaths detected by TRMM, although the simulated maxima were often weaker than observed. Similar patterns of TRMM and RM3 congruent features were evident for each of the 5 summers, 1998 to 2002. The swath during 9–11 August with a maximum of >30 mm at 7° W was reproduced by RM3/NCPR2, but not by RM3/ERA-I, demonstrating occasional impacts of the LBC. This was quantified by the statistics presented in Table 1.

A comparison of Hovmöller time–longitude distributions (such as in Fig. 5) of RM3 precipitation to corresponding TRMM values was made for each of the 3 simulations and each of the 5 JJAS seasons. Table 1 gives some statistics of these comparisons. Note that each data set includes 12 566 values (122 d × 103 longitude grids). Correlations between corresponding Hovmöller distributions reflected model versus TRMM precipitation congruence of longitudinal variability on a given day during 1 June to 30 September, and the congruence of time variability along each longitude, 20° W to 25° E. Correlation coefficients for RM3/ERA-I versus TRMM ranged from 0.76–0.87, while they were consistently higher for RM3/NCPR2 versus TRMM, ranging from 0.89–0.97. Model minus TRMM differences of the means (bias) were positive for each simulation for each season, with a maximum of about 2 mm d^{-1} for ERA-I forcing in 2001. The bias for the NCPR2 forcing was lower than for ERA-I forcing in 3 of the 5 yr. The standard deviation of model precipitation rates was consistently lower than for TRMM observations, because RM3 generated fewer extreme maxima and minima, compared with TRMM, as is evident in Fig. 5. RM3/ERAdegr produced many more near-zero precipitation rates (Fig. 5D), but maxima within the swaths were much too weak. Accordingly, this simulation registered the lowest correlations, negative bias and a standard deviation that was only 74–84% of the control values (Table 1). Fig. 6 shows the cumulative probability density curves for daily precipitation rates during JJAS 2002, from the corresponding time–longitude distribution. Probability density curves for the other 4 yr are quite similar. Fig. 6 shows that the TRMM distribution included more extreme values at both the high and low ends of

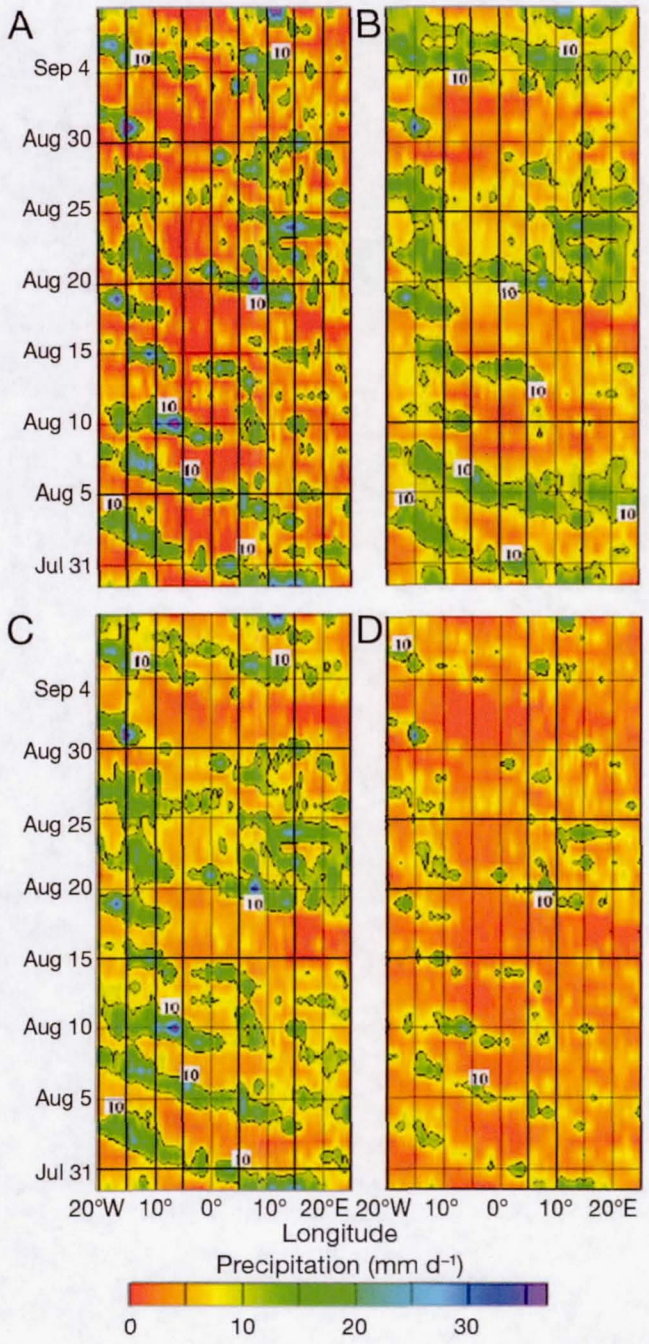

Fig. 5. Time–longitude Hovmöller distributions of daily precipitation (mm), 30 July–8 September 2002, averaged between 5 and 15° N at each longitude. (A) TRMM, (B) RM3/ERA-I, (C) RM3/NCPR2 and (D) RM3/ERAdegr

its population than the model-generated data. For example, the highest 5% of TRMM data achieved a range of 18–28 mm d^{-1}, while the highest 5% of model data ranged from 15–24 mm d^{-1}. Similarly, approximately 20% of TRMM values were <1 mm d^{-1}, while only about 4% of model values were that low. The positive bias of model results (Table 1) in each year was a consequence of too few near-zero simulated precipitation rates. NCPR2 forcing produced a correctly higher standard deviation of precipitation rates in 4 of the 5 years. Fig. 6 shows that this forcing generated slightly higher maxima than ERA-I forcing. However, forcing with the degraded resolution ERA data shifted the upper 50% of values considerably toward lower values compared with the other data sets. In summary, the RM3 simulates westward-propagating precipitation maxima during JJAS, presumably associated with AEWs or imbedded squall lines, that follows the same trajectories and timing as TRMM-observed maxima. However, RM3 daily rainfall rates occupied a narrower range, evidenced by standard deviations that were only 55–77% of corresponding TRMM standard deviations. NCPR2 forcing achieved somewhat better results regarding simulated meridional and zonal movement of precipitation maxima, despite the negative influence of low horizontal resolution.

4.2. Circulation

Simulation of the mid-tropospheric African Easterly Jet (AEJ) is crucial for modeling studies of the summertime WAM. African Easterly Waves (AEWs) develop from the vertical wind shear below the jet core —westward-directed (easterly) shear that is directly proportional to the strength of the meridional temperature gradient in the lower troposphere between the latitude of the rain belt and the Sahara. The altitude of the AEJ core is determined by a reversal to eastward-directed (westerly) wind shear in the mid-troposphere corresponding to the reversal of the meridional temperature gradient above the 600 mb level. Simulation errors in the 3-dimensional temperature structure therefore create errors in the simulation of the AEJ. Conversely, a realistically modeled AEJ implies reasonably modeled thermal structures because of the hydrostatic relationships between temperature gradients and circulation. Fig. 7A–E are cross-sections of JJAS 1998–2002 mean zonal wind along 0° longitude, each showing an AEJ core at 600 mb, near-surface monsoon westerlies (925 mb) and the Tropical Easterly Jet (200 mb). All 5 versions in Fig. 7 place the AEJ core at 600 mb near 12–15° N, with the NCPR2 position some 2° more northerly than the others. The core speed of the AEJ based on either reanalysis (Fig. 7A,B) was about −12 m s^{-1}, while low-level monsoon westerlies over WA reached about 2 m s^{-1}. ERA-I

Table 1. Statistics comparing TRMM versus RM3/ERA-I, RM3/NCPR2 and RM3/ERAdegr time–longitude distributions of daily rainfall, 1 June–30 September, 20° W–25° E, averaged over 5–15° N

	r			Bias			SD			
	RM3/ERA-I vs. TRMM	RM3/NCPR2 vs. TRMM	RM3/ERAdegr vs. TRMM (mm d^{-1})	RM3/ERA-I minus TRMM (mm d^{-1})	RM3/NCPR2 minus TRMM (mm d^{-1})	RM3/ERAdegr minus TRMM (mm d^{-1})	RM3/ERA-I (mm d^{-1})	RM3/ NCPR2 (mm d^{-1})	RM3/ ERAdegr (mm d^{-1})	TRMM (mm d^{-1})
1998	0.87	0.89	0.72	+0.3	+0.5	−2.9	4.3	4.1	3.6	7.4
1999	0.83	0.97	0.70	+1.2	+0.2	−2.9	4.3	5.2	3.5	7.1
2000	0.77	0.95	0.67	+1.6	+0.4	−2.7	3.9	4.5	3.0	6.2
2001	0.80	0.96	0.67	+2.1	+0.5	−2.6	4.1	4.6	3.1	6.1
2002	0.76	0.93	0.69	+1.6	+1.6	−2.5	4.2	4.8	3.1	6.2

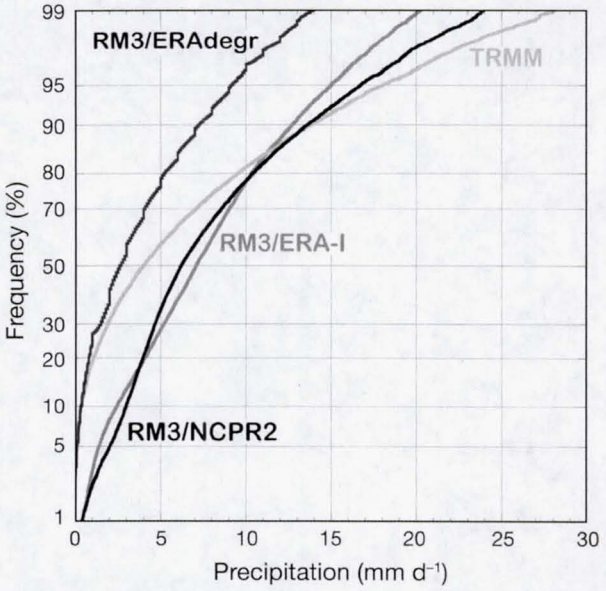

Fig. 6. Cumulative frequency of daily precipitation rates averaged over 5–15° N for Hovmöller time–longitude distributions during JJAS 2002 for TRMM and 3 simulations. Note that *y*-axis scale is adjusted for normal distribution

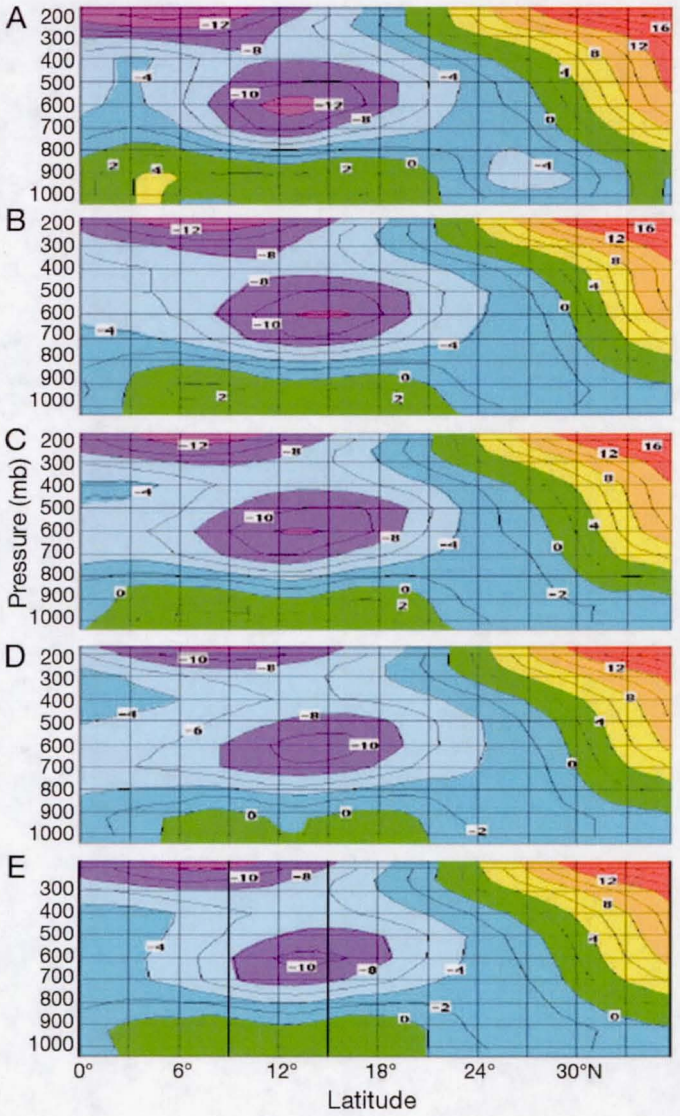

Fig. 7. Pressure–latitude cross-sections of the zonal wind (m s^{-1}) along 0° longitude for JJAS 1998–2002. (A) ERA-I, (B) NCPR2, (C) RM3/ERA-I, (D) RM3/NCPR2 and (E) RM3/ERAdegr

had a core of stronger near-surface westerlies and a correspondingly deeper monsoon layer at 4° N (over the Gulf of Guinea). Zonal wind shear south of the AEJ was slightly weaker for the simulations than for ERA-I, otherwise simulated vertical and horizontal shears were consistent with both reanalyses. The 2 simulations forced by low-resolution LBCs (Fig. 7D,E) produced lower AEJ core speeds, shallower monsoon layers and weaker near-surface monsoon westerlies, compared with both reanalyses. The ERA-I maximum at 4° N was not simulated by any of the 3. At other latitudes, the RM3/ERA-I monsoon layer of westerlies and its northward penetration to about 22° N were quite realistic.

Fig. 8 shows JJAS 1998–2002 means of the zonal wind component at 925 mb (u9) for ERA-I, NCPR2,

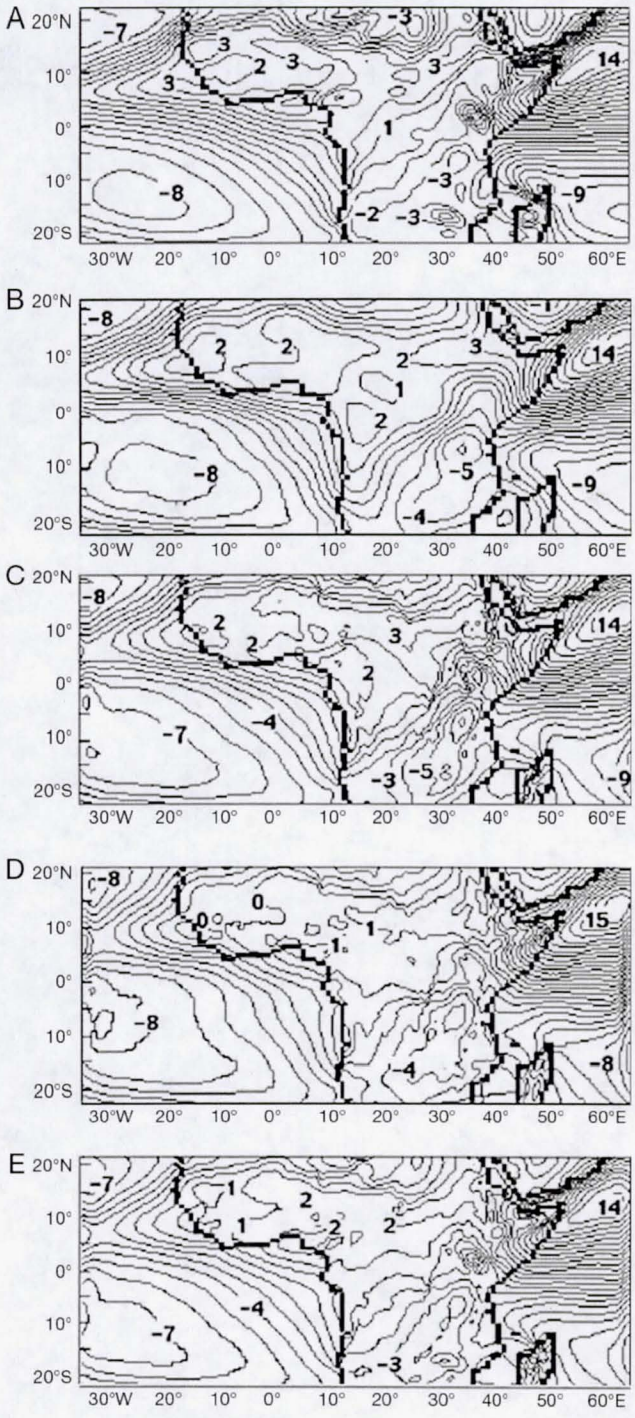

Fig. 8. JJAS 1998–2002 zonal wind components at 925 mb (m s^{-1}). (A) ERA-I, (B) NCPR2, (C) RM3/ERA-I, (D) RM3/NCPR2 and (E) RM3/ERAdegr

RM3/ERA-I, RM3/NCPR2 and RM3/ERAdegr. RM3/ERA-I reproduced the main centers of zonal maxima and minima that were given by the reanalyses. Both reanalyses indicated u9 in excess of 2 m s^{-1} over portions of WA, and RM3/ERA-I reproduced this feature. NCPR2 westerlies were slightly weaker than those of ERA-I, but RM3/NCPR2 managed only weak westerlies, and those only east of 0° longitude, for example, over the Cameroon coast and the Sudan. RM3/ERAdegr produced monsoonal westerlies of intermediary strength. All simulations did, however, produce easterly trade winds over the Atlantic, easterly Harmattan winds over the Sahara and the very strong westerly maximum of the Somali Jet.

The greater northward penetration of the monsoonal rain belt and the deeper monsoonal layer for RM3/ERA-I (shown in Fig. 7) were consistent with its stronger u9 and stronger (JJAS mean) meridional circulation at 925 mb (v9) (Fig. 9). Specifically, RM3/ERA-I v9 of 2–3 m s^{-1} over WA were quite realistic (Fig. 9C) compared to reanalysis (Fig. 9A,B), while RM3/NCPR2 (Fig. 9D) and RM3/ERAdegr (Fig. 9E) featured v9 that were about 1 m s^{-1} slower.

Monsoon southwesterlies at 925 mb were appropriately stronger for both simulation ensembles driven by ERA-I, in contrast to the NCPR2-forced ensemble. However, degradation of the ERA-I LBCs did diminish the southwesterlies over WA.

Transient AEWs during JJAS cause periodic fluctuations in the meridional wind in the lower troposphere over WA and the adjacent Atlantic Ocean (Burpee 1972, Druyan et al. 1996). The RM3 reproduced many of the observed fluctuations by propagating and developing incipient perturbations introduced at the boundaries by the forcing data. Fig. 10 shows a time series of the 700 mb meridional wind component (v7) at 13° N, 2° E (approximately the location of the radiosonde at Niamey, Niger), between 1 July–31 August 2002, for both reanalyses and the RM3/ERA-I and RM3/NCPR2 simulations. The corresponding time series for RM3/ERAdegr, which was almost perfectly correlated with the control, is not shown in order to improve clarity. All 4 time series included many well-defined transitions from strong northerlies to strong southerlies, such as, for example, transitions associated with the passage of 2 high-amplitude AEWs between 30 July and 9 August. (This contributed to a strong spectral peak at a period of 5.3 d, as discussed below, this section) NCPR2 data registered most of the strongest southerly (positive) maxima and some of the strongest northerly (negative) maxima.

Statistical comparisons were made between v7 time series at 13° N, 2° E for the other 4 yr of the study, and at 4 other locations affected by traversing AEWs (5° N, 5° W; 16° N, 15° W; 15° N, 10° W; 18° N, 25° W). Mean correlations (r) and standard deviations

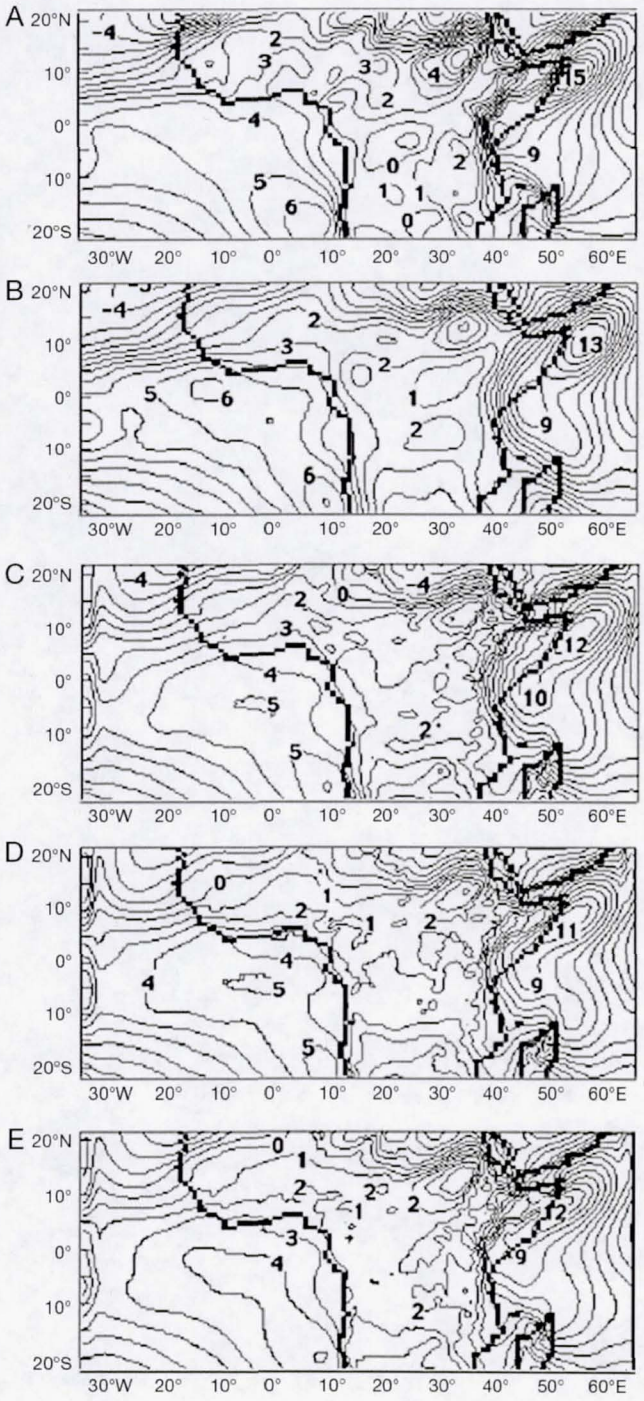

Fig. 9. JJAS 1998–2002 meridional wind components at 925 mb (m s^{-1}). (A) ERA-I, (B) NCPR2, (C) RM3/ERA-I, (D) RM3/NCPR2 and (E) RM3/ERAdegr

over JJAS 1998–2002 are given in Table 2 for 13° N, 2° E. Consistent with the example shown in Fig. 10, the highest r-values were achieved between each simulated v7 time series versus the corresponding v7 in its forcing data set. The v7 time series for RM3/NCPR2 correlated much better with NCPR2 than with ERA-I, but v7 for the control and for RM3/ERAdegr correlated well with both reanalyses. Table 2 indicates a relatively low r between the 2 reanalyses, for which 5 yr mean r-values ranged from 0.55 to 0.64 at the 5 locations. Note that the standard deviation of simulated v7 at 13° N, 2° E was only about 71% of the standard deviations for the corresponding reanalysis v7 (Table 2). At the 5 locations, the 5 yr mean standard deviation of the RM3/ERA-I-simulated v7 ranged from 68 to 79% of the corresponding ERA-I value, indicating that simulated time variability was consistently lower than that given by both reanalyses.

Results reflected different impacts of the alternative LBCs and mutual incongruities between the reanalyses. RM3 simulations forced by reanalysis reproduced the observed timing of AEWs at a given location because of relevant information supplied in the LBCs. These results show that the 2 reanalysis products used here supplied enough of the same relevant information to allow the RM3 to generate most of the same AEWs. The lower standard deviations of the simulated v7 indicate that the RM3 dampened v7 variability. Degrading the resolution of ERA-I LBCs produced an even greater damping of v7 variability, but did not adversely affect the timing of AEWs, as evidenced by high correlations of the RM3/ERAdegr v7 with all other data sets (Table 2).

The periodicity can be detected by spectral analysis of v7 time series. Fig. 11 shows sample spectra for the same location as in Fig. 10, based on v7 time series recorded 4 times daily for JJAS 2002. Druyan et al. (1996) showed v7 spectra for Niamey radiosonde data for July–August 1987 and 1988, which featured spectral peaks at periods of 3.8 to 4.0 d and 5.2 d. The spectrum in Fig. 11A from ERA-I data included a sharp, rather strong peak at 5.3 d, and a lower, but significant peak at 4.3 d. Fig. 11B depicts the v7 spectrum at the same location for NCPR2 data, featuring an even stronger peak at 5.3 d, and additional significant peaks at 4.9, 4.3 and 2.9 d. The 5.3 d spectral peak was also prominent in Fig. 11C and D for the RM3/ERA-I and RM3/NCPR2 simulations, respectively, in addition to lower peaks at 4.9 and 4.3 d. However, the main spectral peaks for these simulated v7 spectra were only 69–78% of the corresponding peak for the ERA-I forcing data (Fig. 11A), probably owing to weaker simulated v7 maxima and minima, as discussed above for Fig. 10. NCPR2 forcing additionally dampened the primary spectral peak, as did forcing with the low-resolution ERA

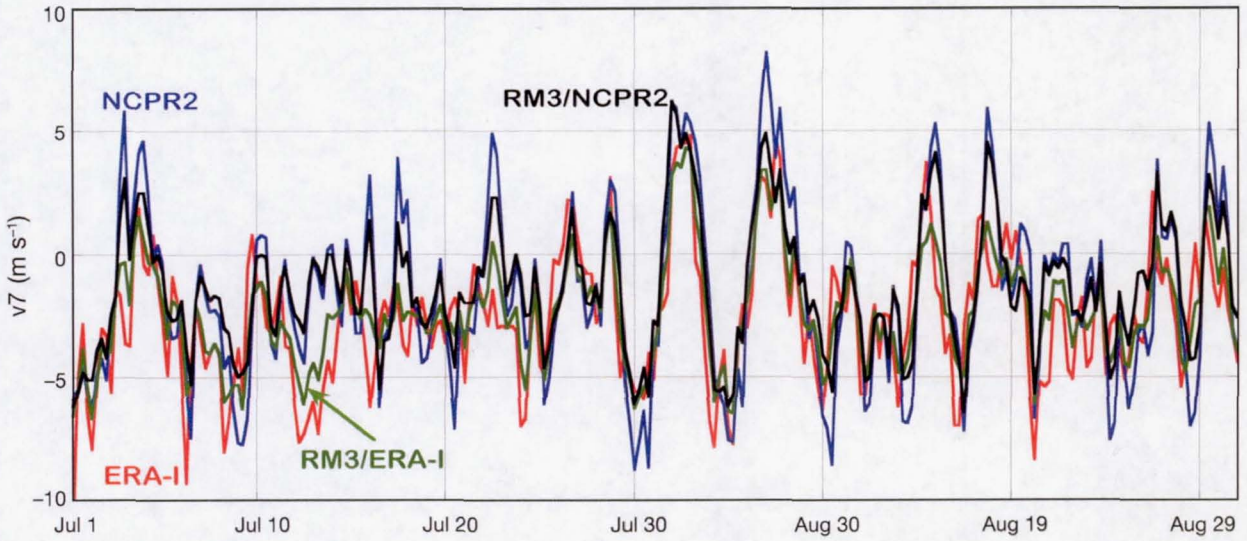

Fig. 10. Time series recorded 4 times daily of meridional wind at 700 mb (v7) at 13° N, 2° E, 1 July–31 August 2002. ERA-I (red), NCPR2 (blue), RM3/ERA-I (green) and RM3/NCPR2 (black)

Table 2. Correlation coefficients and standard deviations (SD) averaged over 1998–2002, for v7 JJAS time series at 13° N, 2° E

	ERA-I	NCPR2	RM3/ ERA-I	RM3/ NCPR2	RM3/ ERAdegr
ERA-I	1.0	0.63	0.91	0.63	0.88
NCPR2	–	1.0	0.86	0.96	0.87
RM3/ERA-I	–	–	1.0	0.86	0.97
RM3/NCPR2	–	–	–	1.0	0.88
RM3/ERAdegr	–	–	–	–	1.0
SD	3.1	3.1	2.2	2.2	2.0

data. Examination of v7 spectra for other years showed that spectral peaks occurred at different periods in different years, but RM3 spectra had peaks that were consistent with the driving data. The spectra for RM3/ERAdegr had peaks at the same periods as the control, but the significant ones averaged about 20% weaker.

The foregoing analysis of v7 time series and the spectral analysis demonstrated that the RM3 model simulated v7 variability that mirrors the driving analyses. This also implied that RM3 creates AEW activity over WA that parallels reanalysis. Moreover, since downscaling each reanalysis produced time series of v7 with spectral peaks at matching periods, both sets of LBCs were presumed to contain the conditions for initiating each wave, usually with the same timing.

Fig. 12 shows Hovmöller time–longitude distributions of relative vorticity, based on the zonal gradient of v7 ($\zeta = \delta v/\delta x$), here averaged between 5 and 15° N. Druyan & Fulakeza (2011) previously showed that this representation of vorticity conveniently tracks wave perturbations imbedded in the mid-tropospheric easterly circulation over WA. (The second term of relative vorticity, $-\delta u/\delta y$, was consistently positive in this regime of strengthening easterlies toward the north, while ζ was positive near wave troughs.) Thorncroft et al. (2007) created a similar time–longitude diagnostic for AEW trajectories by plotting 700 mb curvature vorticity. The diagonal swaths of positive ζ (amber/brown/red) in Fig. 12 showed the westward propagation of AEW cyclonic troughs across WA during July–August 2002. The positive ζ swaths alternated with negative extremes (green/blue) that represented the anti-cyclonic circulations between AEWs. All 5 Hovmöllers indicated many of the same AEWs, with the same timing and westward progress of ζ centers. However, differences were apparent between the distributions derived from ERA-I (Fig. 12A) versus NCPR2 (Fig. 12B), as well as from the simulations. For example, swaths of positive ζ for the intervals 23–31 July and 9–13 August showed more continuity in NCPR2 than in ERA-I. Differences were also reflected by the statistics given in Table 3. Although both reanalysis data sets probably shared much of the same observational data, they were produced by 2 different models and archived at very different horizontal resolutions (0.75° versus 2.5°). Each reanalysis represented its version of the actual circulation, so any advantage of one over the other was difficult to validate.

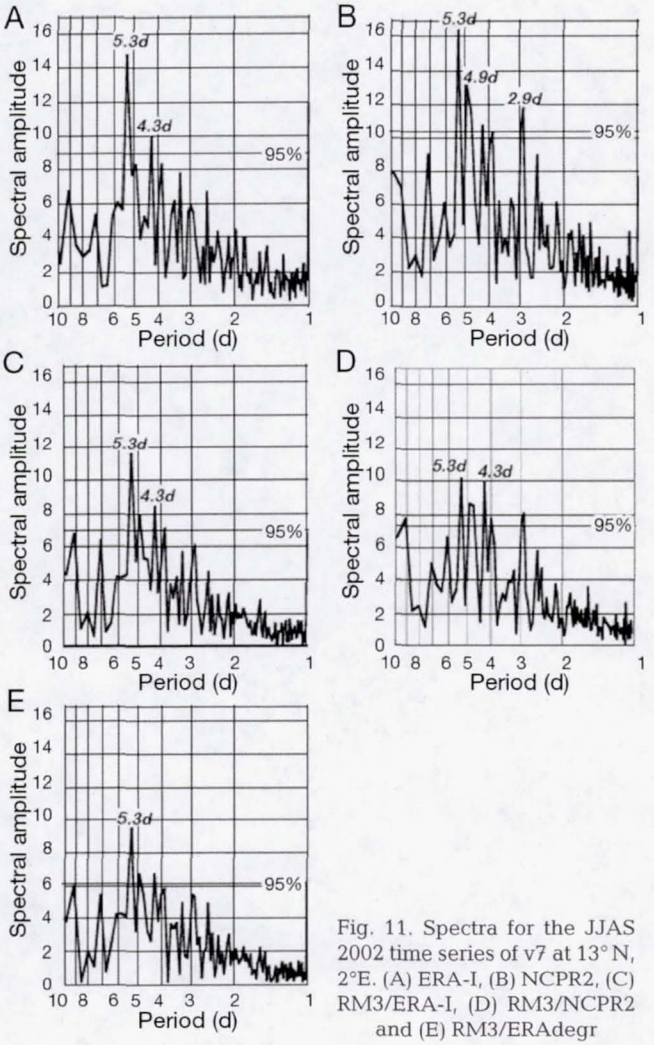

Fig. 11. Spectra for the JJAS 2002 time series of v7 at 13° N, 2°E. (A) ERA-I, (B) NCPR2, (C) RM3/ERA-I, (D) RM3/NCPR2 and (E) RM3/ERAdegr

The most glaring discrepancy of the RM3/ERA-I-simulated Hovmöller distribution of ζ (Fig 12C) compared to reanalysis was its dampened maxima, consistent with the dampened v7 fluctuations of the control, discussed earler in this section. Otherwise, the control pattern followed the ERA-I data more closely than the NCPR2 data. RM3/NCPR2 (Fig. 12D), on the other hand, achieved more extreme ζ maxima than the control, consistent with the forcing analysis. RM3/ERAdegr (Fig. 12E) reproduced the control pattern quite well, but many maxima were slightly weaker.

Correlations were computed between the time–longitude distributions of ζ for each of the 2 reanalyses and 3 simulations for each JJAS season. In order to compute the correlations, each data set was interpolated to the RM3 grid at 0.44° spacing. The 5 yr mean correlations are given in Table 3. The interannual range of correlations was quite narrow, 0.04 or less. The RM3/ERA-I Hovmöller distribution featured most of the ζ maxima and minima computed from the ERA-I data set, achieving a 5 yr mean correlation of 0.84. Control simulation storm tracks were slightly less congruent with NCPR2 ζ, and the 5 yr mean correlation was accordingly reduced to 0.72. Vorticity trajectories implied by ERA-I and NCPR2 data were even more weakly correlated with each other (r = 0.30) than corresponding v7 time series (see Table 2), emphasizing the different daily circulations in each reanalysis. The time–longitude ζ pattern produced by RM3/NCPR2 was nearly perfectly correlated with its own forcing data (r = 0.95), but only weakly correlated with the ERA-I field (r = 0.30). If the high-resolution ERA-I provided a better representation of actual circulation than NCPR2, then the RM3 time–longitude ζ distribution produced with ERA-I as LBCs came much closer to the actual distribution than using NCPR2 forcing and was slightly closer than the simulation with ERA degraded resolution forcing. Although most AEWs develop and are amplified well within the RM3 domain (Druyan et al. 2008), LBCs were shown to have a large impact on the evolving circulation, perhaps via incipient waves introduced along the boundaries. In each case, RM3 grew and propagated AEWs in close agreement with reanalysis observational evidence, a conclusion supported also by the spectral analysis above.

5. CONCLUSIONS

The RM3 regional atmospheric model was driven in parallel simulations by LBCs recorded 4 times daily from ERA-I and NCPR2 reanalyses, 1 January to 31 December for 5 consecutive years, 1998–2002. These are the earliest 5 yr for which TRMM precipitation observations were available for validation of model simulations. ERA-I forcing data were provided by the CORDEX project at a 0.75° grid spacing, while NCPR2 was gridded at 2.5°. A third 5 yr ensemble was simulated between 1 May and 6 October, using ERA-I LBCs at a horizontal grid resolution of 2.5°. RM3 was integrated at 28 vertical levels, with a horizontal grid spacing of 0.44°. The model domain was centered over Africa, but included large portions of the Atlantic Ocean and the western Indian Ocean. The high resolution of ERA-I data, combined with the ambitious CORDEX plan to simulate multiple decades, was resource intensive, so it was instructive to examine the relative advantages of ERA-I. This study evaluated whether there are benefits to forcing RCM simulations over Africa with one or the other of the reanalysis data

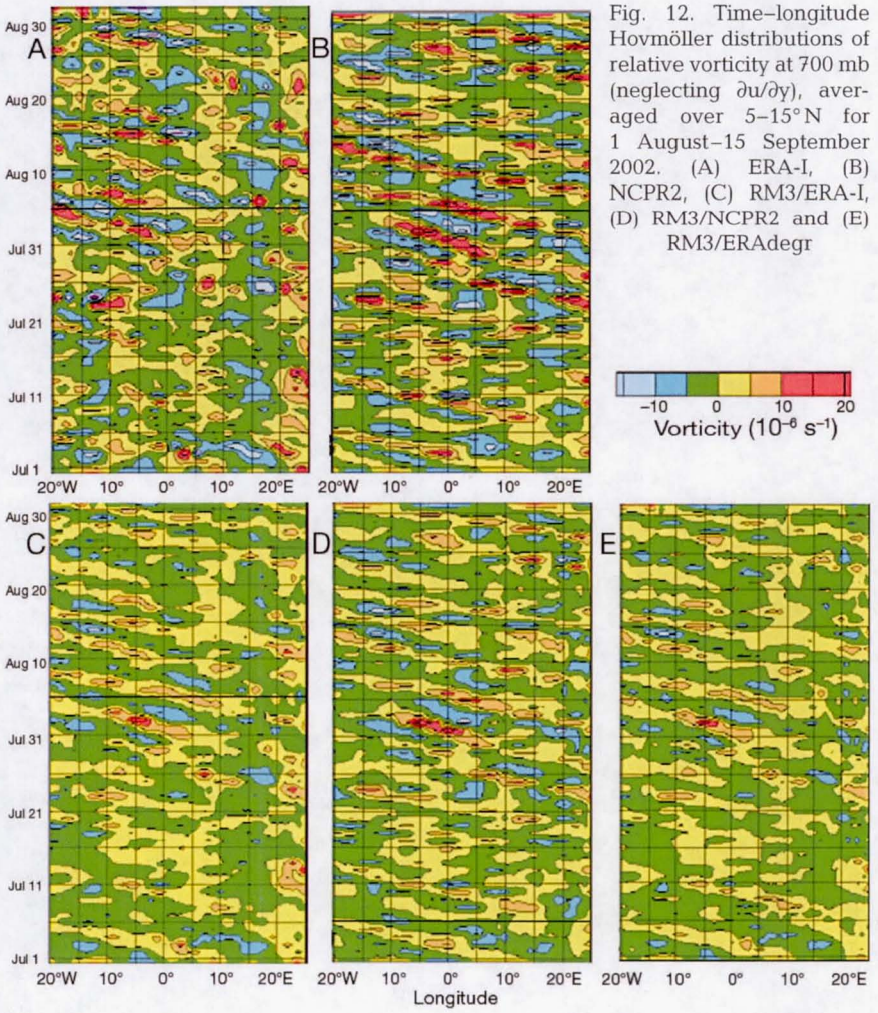

Fig. 12. Time–longitude Hovmöller distributions of relative vorticity at 700 mb (neglecting $\partial u/\partial y$), averaged over 5–15° N for 1 August–15 September 2002. (A) ERA-I, (B) NCPR2, (C) RM3/ERA-I, (D) RM3/NCPR2 and (E) RM3/ERAdegr

Table 3. Mean correlations between time–longitude Hovmöller distributions of 12:00 h (UT) vorticity, 1998–2002. All correlations are significant at the 99% confidence level

	ERA-I	NCPR2	RM3/ ERA-I	RM3/ NCPR2	RM3/ ERAdegr
ERA-I	1.0	0.30	0.84	0.30	0.77
NCPR2	–	1.0	0.72	0.95	0.76
RM3/ERA-I	–	–	1.0	0.70	0.94
RM3/NCPR2	–	–	–	1.0	0.77

sets. The downscaling spatial resolution ratio using ERA-I was 1.7:1 (0.75:0.44), and, by using NCPR2, it was 5.7:1 (2.5:0.44). In addition, there were intrinsic differences in the 2 reanalyses owing to their different models and data assimilation schemes. Most of the prior downscaling experience using the RM3 was based on NCPR2 and NCPR1 LBCs on the 2.5° grid.

All RM3 simulations recreated the observed annual cycle of precipitation rates over the northern WA area. WA precipitation was overestimated by the ERA-I-forced control simulations, while NCPR2 forcing produced an annual cycle that perfectly followed the TRMM data. On the other hand, degrading the resolution of ERA-I LBCs caused unrealistic reductions in WA summer rainfall.

Some features of the August minus January precipitation difference distribution were better reproduced by the control, and others, better by NCPR2 forcing. Similarly, each simulation ensemble captured many centers of JAS 1999 minus JAS 2002 precipitation differences, but the control produced a better representation of the positive differences over the Sahel. The control simulation ensemble (ERA-I forced) produced excessive Sahel rainfall during the pre-onset period and spread moderate precipitation rates too far north over WA during the summer. The more moderate precipitation rates produced with NCPR2 forcing created a very realistic northward migration of the rain band, including a pre-onset break in the heavy rainfall connecting the jump from 5 to 10° N.

The RM3 simulations reproduced time–longitude swaths of precipitation, identified as 'footprints' of AEWs, that closely followed TRMM observations. These Hovmöller distributions spanning JJAS correlated better with TRMM for the NCPR2-forced runs (r = 0.94 for 5 seasons) than for the ERA-I-forced simulations (r = 0.81). The simulations based on the resolution degraded ERA-I forcing produced Hovmöller precipitation distributions with much lower correlations against TRMM (r = 0.69).

The control ensemble simulated the most realistic AEJ and near-surface monsoon southwesterlies during JJAS. NCPR2 forcing and degraded resolution ERA-I LBCs unrealistically slowed the AEJ and the onshore 925 mb circulation over WA.

It was clear that ERA-I and NCPR2 differed in many details, even though both represented some version of the actual atmospheric state. For example, their respective time series of v7 were correlated rather imperfectly. Sample spectra computed here of

ERA-I and NCPR2 v7 time series shared the 5.3 d period peak, but differed on the period of the secondary peak. Vorticity swaths of westward-propagating AEWs during JJAS were represented with different timings and intensities by ERA-I and NCPR2. Nevertheless, RM3 simulated very similar vorticity swaths, whether based on ERA-I or NCPR2 forcing. NCPR2 LBCs created realistically stronger 700 mb vorticity maxima, even while simulating a weaker AEJ core than that in the control. However, each simulation ensemble created vorticity swaths well correlated with its driving data.

Differences between reanalyses may have accounted for the somewhat different outcomes in the RM3/ERA-I versus RM3/NCPR2 simulations. Results presented here imply that forcing regional model simulations with ERA-I data, rather than with NCPR2, is not advantageous in every respect, despite the higher resolution of ERA-I. For example, NCPR2 forcing produced RM3 precipitation distributions and propagation of precipitation maxima that were more faithful to TRMM validation. On the other hand, unrealistically weak monsoon circulation and underestimated precipitation rates simulated by RM3/ERAdegr suggest that the high resolution of ERA-I did make a positive contribution to the downscaling.

The current configuration of the RM3 has been optimized over the years to generate reasonable summer rainfall rates over WA with NCPR2 forcing, although this downscaling produces a somewhat sluggish southwesterly monsoon circulation. The ERA-I-forced simulation ensemble achieved realistically stronger southwesterlies that increased moisture convergence, perhaps explaining its excess precipitation. If this is true, the conclusions of the study may be rather model dependant.

Acknowledgements. This research was supported by the US National Science Foundation Grant AGS-1000874 and the NASA Cooperative Agreement NNX11AR63A. TRMM data used in this study were acquired using the GES-DISC Interactive Online Visualization ANd aNalysis Infrastructure (Giovanni) as part of the NASA's Goddard Earth Sciences (GES) Data and Information Services Center (DISC). ERA-I data was provided by the European Center for Medium Range Weather Forecasts, facilitated by the CORDEX project. NCEP/DOE reanalysis 2 data were provided by the NOAA-ESRL Physical Sciences Division, Boulder, Colorado, from their web site at www.esrl.noaa.gov/psd.

LITERATURE CITED

Burpee R (1972) The origin and structure of easterly waves in the lower troposphere of North Africa. J Atmos Sci 29: 77–90

Del Genio A, Yao MS (1993) Efficient cumulus parameterization for long-term climate studies. The GISS scheme. In: Emanuel K, Raymond D (eds) Cumulus parameterization, Vol 24. Monograph Series, American Meteorological Society, Boston, p 181–184

Del Genio A, Yao MS, Kovari W, Lo KW (1996) A prognostic cloud water parameterization for global climate models. J Clim 9:270–304

Denis B, Laprise R, Caya D, Cote J (2002) Downscaling ability of one-way nested regional climate models: the Big-Brother Experiment. Clim Dyn 18:627–646

Druyan L (2011) Studies of 21st century precipitation trends over West Africa. Int J Climatol 31:1415–1424

Druyan L, Fulakeza M (2011) The sensitivity of African easterly waves to eastern tropical Atlantic sea-surface temperatures. Meteorol Atmos Phys 113:39–53

Druyan L, Fulakeza M (2012) Propagation of convective complexes observed by TRMM in the eastern Tropical Atlantic. Open Atmos Sci J 6:1–8

Druyan L, Lonergan P, Saloum M (1996) African wave disturbances and precipitation at Niamey during July–August, 1987 and 1988. Clim Res 7:71–83

Druyan L, Fulakeza M, Lonergan P (2006) Mesoscale analyses of West African summer climate: focus on wave disturbances. Clim Dyn 27:459–481

Druyan L, Fulakeza M, Lonergan P (2008) The impact of vertical resolution on regional model simulation of the West African summer monsoon. Int J Climatol 28:1293–1314

Druyan L, Feng J, Cook K, Xue Y and others (2010) The WAMME regional model intercomparison study. Clim Dyn 35:175–192

Gu G, Adler R (2004) Seasonal evolution and variability associated with the West African monsoon system. J Clim 17:3364–3377

Haensler A, Hagemann S, Jacob D (2011) Dynamical downscaling of ERA40 reanalysis data over southern Africa: added value in the representation of seasonal rainfall characteristics. Int J Climatol 31:2338–2349

Hansen J, Sato M, Nazarenko L, Ruedy R and others (2002) Climate forcings in Goddard Institute for Space Studies SI2000 simulations. J Geophy Res 107:1–37

Hernandez-Diaz L, Laprise R, Sushama L, Martynov A, Winger K, Dugas B (2013) Climate simulation over CORDEX Africa domain using the fifth generation Canadian Regional Climate Model (CRCM5). Clim Dyn 40: 1415–1433

Huffman G, Bolvin D, Nelkin E, Wolff DB and others (2007) The TRMM multisatellite precipitation analysis (TMPA): quasi global, multiyear, combined-sensor precipitation estimates at fine scales. J Hydrometeorol 8:38–55

IPCC (2007) Climate change 2007: synthesis report. Contribution of Working Groups I, II and III to the Fourth Assessment Report of the Intergovernmental Panel on Climate Change. IPCC, Geneva

Jones C, Giorgi F, Asrar G (2011) The coordinated regional downscaling experiment: CORDEX, an international downscaling link to CMIP5. CLIVAR Exchanges 16: 34–39

Kanamitsu M, Ebisuzaki W, Woollen J, Yang SK, Hnilo J, Fiorino M, Potter G (2002) NCEP-DEO AMIP-II Reanalysis (R-2). Bull Am Meteorol Soc 83:1631–1643

Lavaysse C, Flamant C, Janicot S, Parker D, Lafore JP, Sultan B, Pelon J (2009) Seasonal evolution of the WA heat low: a climatological perspective. Clim Dyn 33:313–330

Lélé I, Lamb P (2010) Variability of the Intertropical Front

(ITF) and rainfall over the West African Sudan–Sahel Zone. J Clim 23:3984–4004

Lim YK, Stefanova LB, Chan SC, Schubert SD, O'Brien JJ (2011) High-resolution subtropical summer precipitation derived from dynamical downscaling of the NCEP/DOE reanalysis: How much small-scale information is added by a regional model? Clim Dyn 37:1061–1080

Mitchell T, Jones P (2005) An improved method of constructing a database of monthly climate observations and associated high-resolution grids. Int J Climatol 25:693–712

Nikulin G, Jones C, Giorgi F, Asrar G and others (2012) Precipitation climatology in an ensemble of CORDEX-Africa regional climate simulations. J Clim 25:6057–6078

Paeth H, Thamm HP (2007) Regional modeling of future African climate north of 15° S including greenhouse warming and land degradation. Clim Change 83:401–427

Rosenzweig C, Abramopoulos F (1997) Land-surface model development for the GISS GCM. J Clim 10:2040–2054

Steiner A, Pal J, Rauscher S, Bell J and others (2009) Land surface coupling in regional model simulations of the West African monsoon. Clim Dyn 33:869–892

Sylla M, Coppola E, Mariotti L, Giorgi F, Ruti P, Dell'Aquilla A, Bi X (2010) Multiyear simulation of the African climate using a regional climate model (RegCM3) with high resolution ERA-interim reanalysis. Clim Dyn 35:231–247

Sylla M, Giorgi F, Ruti P, Calmanti S, Dell'Aquila A (2011) The impact of deep convection on the West African summer monsoon climate: a regional climate model sensitivity study. Q J R Meteorol Soc 137:1417–1430

Thorncroft C, Lafore J, Berry G, Roca R, Guichard F, Tomasini M, Asencio N (2007) Overview of African weather systems during the summer of 2006. CLIVAR Exchanges 12(2):18–20

Thorncroft C, Nguyen H, Zhang C, Peyrillé P (2011) Annual cycle of the West African monsoon: regional circulations and associated water vapour transport. Q J R Meteorol Soc 137:129–147

Xue Y, Shukla J (1993) The influence of land surface properties on Sahel climate. I Desertification. J Clim 6: 2232–2245

Editorial responsibility: Filippo Giorgi, Trieste, Italy

Submitted: February 28, 2012; Accepted: January 15, 2013
Proofs received from author(s): April 11, 2013